OPEN ACCESS Freely available online

Journal of Citrus Pathology

Research Article

Applying volumetric electron microscopy to visualize xylem tissue impacted by citrus tristeza virus-induced stem pitting

DJ Aldrich[1], J Kriel[2], R Bester[1,3], JT Burger[1] and HJ Maree[1,3*]

[1]Department of Genetics, Stellenbosch University, Private Bag X1, Matieland 7602, South Africa; [2]Central Analytical Facilities, Microscopy Unit, Stellenbosch University, Cape Town, South Africa; [3]Citrus Research International, PO Box 2201, Matieland, 7602, South Africa

*Correspondence to: hjmaree@sun.ac.za

Citation: Aldrich, D. J, Kriel, J., Bester, R., Burger, J. T, & Maree, H. J. (2024). Applying volumetric electron microscopy to visualize xylem tissue impacted by citrus tristeza virus-induced stem pitting. Journal of Citrus Pathology, 11(2). http://dx.doi.org/10.5070/C411262569 Retrieved from https://escholarship.org/uc/item/5ks4156z

Abstract

Citrus tristeza virus (CTV) causes several disease syndromes in different citrus hosts; namely quick decline, seedling yellows, and stem pitting. CTV-induced stem pitting leads to substantial economic losses in sensitive citrus varieties, including grapefruit. The formation of stem pits has previously been linked to the ability of the virus to colonize xylem tissue outside of its typical phloem limitation, thereby disrupting normal xylem development. The nature of this compromised tissue has not been fully elucidated. In this study, stem pits were characterized at the molecular anatomical level using a combination of techniques to better understand the characteristics of the xylem and phloem tissues impacted by severe pitting. Biological staining was used to visualize CTV-induced stem pitting and was complemented with a novel technology that has not previously been used to study CTV-induced stem pitting, namely serial block-face scanning electron microscopy (SBF-SEM). This proof-of-concept study yielded new insights into the morphology of stem pitting-affected tissue. The utility of SBF-SEM for stem pitting characterization was also demonstrated and an optimized protocol for its application on hard, woody material is presented.

Keywords: CTV, 3DEM, SBF-SEM, Software renderings, Biological staining

Introduction

Stem pitting is a plant disease phenotype that results from the disruption of vascular tissues and is induced by several plant viruses in different woody perennial crops including pome and stone fruit, grapevine, avocado, and citrus (Lott et al., 1962; Welsh and May, 1966; Smith et al., 1973; Brlansky et al., 2002; Marini et al., 2002; Martelli et al., 2007; Dawson et al., 2013). Citrus tristeza virus (CTV), a member of the species *Closterovirus tristezae* and a phloem-limited virus in the family *Closteroviridae*, can cause severe stem pitting in susceptible citrus hosts, including sweet orange, grapefruit and lime (Moreno et al., 2008; Dawson et al., 2013; Folimonova, 2013). Stem pitting has historically been a perplexing citrus disease syndrome to study, and despite considerable effort over many decades, the exact mechanisms of CTV-induced stem pitting in citrus remain unclear (Dawson et al., 2013; Sun and Folimonova, 2019, 2022).

Using green fluorescent protein (GFP)-tagged CTV infectious clones, Tatineni and Dawson (2012) revealed that in cases of severe pitting, the virus was found replicating deep within the woody parts of the plant, in cells that would normally have developed into mature xylem tissue. Mature xylem is predominantly made up of non-living tracheary elements that function for water and mineral transport (Sun et al., 2022) and is not thought to be capable of facilitating CTV replication. The development of stem pits therefore likely involves CTV-induced changes in cellular differentiation, to allow cells that would normally develop into mature xylem tissue, to remain undifferentiated (parenchymatic) and permit virus replication and spread (Tatineni and Dawson, 2012; Sun and Folimonova, 2022). The exact nature of these cells remains to be elucidated and limited information is available on the three-dimensional morphology of xylem tissue impacted by different stem pitting phenotypes. In the case of large, discrete stem pits there are often also

substantial portions of the compromised xylem that do not separate from the woody trunk when peeling the bark layer away. Gaining a better understanding of the morphology of xylem tissue deep within stem pits could provide useful insights into understanding which parts of the differentiation process are impacted by CTV to yield the undifferentiated cells, capable of facilitating CTV replication.

There have been significant advancements made in high-resolution, three-dimensional (3D) imaging technologies based on electron microscopy (EM) in recent years (Smith and Starborg, 2019) which have not yet been applied to stem pitting characterization in citrus. Serial block-face scanning electron microscopy (SBF-SEM) is a three-dimensional electron microscopy (3DEM) approach developed by Denk and Horstmann (2004) to study animal nerve tissues. SBF-SEM instruments utilize a computer-controlled, automated ultramicrotome, housed within the vacuum chamber of a scanning electron microscope for serial sectioning and imaging of a resin-embedded sample (Hughes et al., 2014; Eustaquio et al., 2018; Goggin et al., 2020). A stack of aligned SEM images is generated, which can then be processed into 3D data sets (Hughes et al., 2014). This also allows subsequent segmentation and 3D rendering of structures of interest to suit a particular investigation (Denk and Horstmann, 2004; Goggin et al., 2020). This technology has been effectively employed in studies on soft mammalian tissues (Helmstaedter et al., 2008; Eustaquio et al., 2018; Lewis et al., 2019; Ornelas et al., 2021). However, its application on hard materials in general, including woody plant material, is very limited.

In this proof-of-concept study, the utility of SBF-SEM was evaluated for the morphological characterization of woody tissues impacted by CTV-induced stem pitting. Visual assessments of cell types affected by stem pitting were complemented with biological staining to differentiate tissue based on lignin content, thereby facilitating the potential classification of cell types within stem pits.

Materials and Methods

Plant material and growth conditions

Stem pits were evaluated in the sensitive stem pitting indicator host, 'Mexican' lime (*C.* × *aurantifolia* (Christm.) Swingle) (Garnsey et al., 1987; Tatineni and Dawson, 2012). Plants were infected with CTV isolate T3-KB (genotype T3) via grafting of infected bark patches from a 'Mexican' lime source plant to induce stem pitting. Plants were pruned and stem sections were sampled after nine months of re-growth to allow sufficient time for stem pitting development. Plants were established in a soil mixture of 50% sand, 25% coir, and 25% vermiculite, in plastic pots (10.2 X 24.1 cm) and maintained in a climate-controlled greenhouse with natural light and temperatures ranging between 22°C and 28°C. For fertilization, pots were supplemented with Osmocote controlled release fertilizers (Osmocote Pro 5-6M, Johannesburg, GT, South Africa) via topical application.

Thin sectioning

Stem portions (~0.6 cm in diameter and 1 cm in length) were sampled and trimmed further using a single-edge razor blade. Samples were then placed onto small cork tiles in the correct orientation for transverse sectioning. Stem sections were covered in tissue freezing media (Leica Biosystems, IL, USA) and submerged into pre-cooled (using liquid nitrogen) isopentane until fully frozen. Frozen samples were then placed in the pre-chilled chamber of the Leica CM1860 cryostat microtome (Leica Biosystems, IL, USA) and equilibrated to -20°C for cutting. Sectioning was performed at a thickness of 20 µm. Thin sections were mounted onto glass slides and kept cold for further processing.

Biological staining

Biological stains were applied to 'Mexican' lime thin sections to differentiate cell types in stem pits. Safranin O, a basic dye, stains lignin irrespective of cellulose presence, whereas Alcian Blue (similar to Astra Blue) is a phthalocyanine dye that stains cellulose only in the absence of lignin (Srebotnik and Messner, 1994). This complementary staining procedure, therefore, enables clear differentiation of cell types based on cell wall lignin content by staining different shades of blue or red. A 1% aqueous Safranin O (Sigma-Aldrich, color index 50240; St. Louis, MO, USA) primary stain was used in combination with a 1% aqueous Alcian Blue 8GX (Sigma-Aldrich, color index 74240; St. Louis, MO, USA) counterstain to identify lignification differences between cell types. Samples were stained with Safranin O for 5 minutes, after which the stain was removed, and sections were washed in a series of ethanol (EtOH) steps (30%, 50%, and 70%). Following the 70% EtOH step, sections were stained with Alcian Blue 8GX for 5 minutes. The same wash steps were applied after the counterstain was applied, with an additional 3-minute 100% EtOH step to dehydrate the sections for visualization. Stained sections were visualized and imaged using a Nikon Eclipse E400 light microscope (Nikon, Amstelveen, Netherlands) with an affixed Pixelink microscope camera (Pixelink, Navitar, Rochester, NY, USA).

Serial block face scanning electron microscopy sample preparation

The Thermo Fisher Apreo Volumescope serial block face scanning electron microscope (SBF-SEM) was used to investigate the three-dimensional morphology of xylem tissue impacted by stem pitting. Individual stem pits were hand-sectioned using a single-edge razor blade. The bark layers were removed in each case and samples were imaged via low-vacuum scanning electron microscopy for region finding. For this, uncoated samples were placed on SEM stubs with double-sided carbon tape and acquired with the Volumescope Dual Back-Scatter Detector (VS-DBS) at a vacuum of 0.5 mbar, with a beam strength of 2 kV and current of 0.1 nA.

Samples were fixed for 24 hours at 4°C with a mixture of 2.5% glutaraldehyde and 4% formaldehyde in a 0.1 M phosphate buffer. Thereafter, incubation with 2% reduced osmium tetroxide (OsO4) was conducted for 60 minutes on ice. This mixture consisted of a 1:1 ratio of 4% OsO4 (SPI S-02600-BA; SPI, West Chester, PA, USA) and 3% potassium ferricyanide (Sigma-Aldrich P-9387; St. Louis, MO, USA). This was followed by a 20-minute incubation with thiocarbohydrazide (TCH) (Sigma-Aldrich 88535, St. Louis, MO, USA) at room temperature, 30-minute incubation with aqueous osmium tetroxide at room temperature and overnight incubation with 1% uranyl acetate (Agar Scientific, Essex, UK) at 4 ˚C. Samples were washed three times with distilled water (dH2O) between each incubation step. (Tapia et al., 2012)

After overnight incubation, dehydration in an ethanol series of increasing concentrations (20%, 50%, 70%, 90%, 100%) was conducted for 10 minutes each on ice, followed by two rounds of 100% EtOH dehydration at room temperature. Resin infiltration was performed in a series of 2-hour incubation steps at room temperature, using increasing concentrations (25%, 50% and 75%) of EPON resin (SPI-Pon 812 S-02660-AB; SPI, West Chester, PA, USA) diluted in acetone. A final infiltration step with 100% EPON resin was performed overnight on a rotator (R5010 rotating mixer, Benchmark Scientific, Sayreville, NJ, USA). Lastly, samples were transferred to embedding mounts and placed in an oven at 60°C for 2 days to allow for appropriate polymerization and hardening of the resin.

Following resin embedding, the resin block was trimmed to a region of interest (ROI) of 0.7 x 0.7 x 1 mm with a Leica UC7 ultramicrotome system (Leica Microsystems, Austria) using a glass knife. The trimmed block was then mounted on an ultramicrotome stub using conductive silver epoxy (SPI, S-05000-AB; SPI, West Chester, PA, USA). To facilitate the hardening of the epoxy, samples were transferred to an oven for 2 hours at 60°C. Excess epoxy was trimmed away, and fine cutting of the resin block continued with the ultramicrotome, using a diamond knife (Diatome, Hatfield, PA, USA). The block face was then sputter coated with 50 nm gold/palladium (Denton Desk V, Moorestown, NJ, USA) followed by another round of ultramicrotome sectioning (100 nm thin sections) to expose the sample block face. Additional sectioning was conducted for precise region confirmation, which entailed catching the 100 nm sections onto silicon nanowafers for high-resolution SEM, before continuing with SBF acquisition.

Serial block face scanning electron microscopy

The ultramicrotome stub was placed into the ultramicrotome attachment of the Apreo Volumescope SBF-SEM (Thermo Fisher, Netherlands), and eucentric calibration of the diamond knife to the block face was conducted. After confirming the alignment of the sample to the knife, the sample chamber was closed and pumped to the appropriate vacuum. Image acquisition was conducted at an adjusted chamber pressure of 0.5 mbar to compensate for excessive charging of the resin. Under a lowered chamber vacuum pressure of 0.5 mbar, the VolumeScope Dual Back Scatter (VS DBS) detector was implemented, using a voltage of 3 kV and probe current of 0.2 nA. Region finding and beam energy alignment were conducted using Xt Microscopy and Maps 3.9 software (Thermo Fisher, Netherlands). A z-width of 100 nm was deemed appropriate as cutting thickness. Sample polishing commenced at 100 nm thickness for 100 slices following eucentric positioning. Thereafter, volumetric electron microscopy data was acquired for a total of 200 slices using the VS-DBS detector at a pixel resolution of 3840 x 2160 with a scan speed of 2 µs.

For 3D rendering, image stacks were aligned and pre-processed in Amira (version 2019.3) (Thermo Fisher, Netherlands) and exported as tiff stacks. Manual segmentation was conducted on tiff stacks using Ilastik (version 1.3.3post3) (https://www.ilastik.org/). Once areas of interest were identified, pixel-predicted maps of these structures were exported as hdf5 files into Fiji (ImageJ2 version 2.3.0/1.53q) (https://imagej.net/) for the creation of binary files that could be identified as 3D volumes in Amira. All final rendering and overlays with the original image stacks were conducted in Amira.

Results and discussion

Biological staining for lignification differences

Viruses require the cellular machinery of living cells for their replication, assembly, and protein synthesis (Pallas and García, 2011; Sun et al., 2022). Mature xylem tissue is not thought to be capable of facilitating CTV replication as it mostly comprises non-living tracheary elements (Tatineni and Dawson, 2012). For CTV replication to occur within the tissue that comprises stem pits, the cells would, therefore, be expected to be living and distinguishable from the unaffected neighboring xylem tissue. The cell walls of living, parenchymatic tissue would be significantly less lignified compared to the highly organized and lignified secondary cell walls of the surrounding xylem tracheids and vessel elements (Sun and Folimonova, 2022). By utilizing the biological stain and counterstain system of Safranin O and Alcian Blue 8GX, cell types could be differentially stained based on their cell wall lignin content.

Firstly, the impact of the stem pits on the phloem-associated cells was visualized via biological staining of thin sections. Fig. 1 shows the comparison of phloem elements in unaffected (Fig. 1a) and pitted (Fig. 1b) portions of the T3-KB infected ‘Mexican’ lime plant. Stem pitting did not appear to have an impact on cells within the cortex layer towards the periphery of the bark layer, as the cells appeared similar in both pitted and unpitted portions of the stem (Fig. 1).

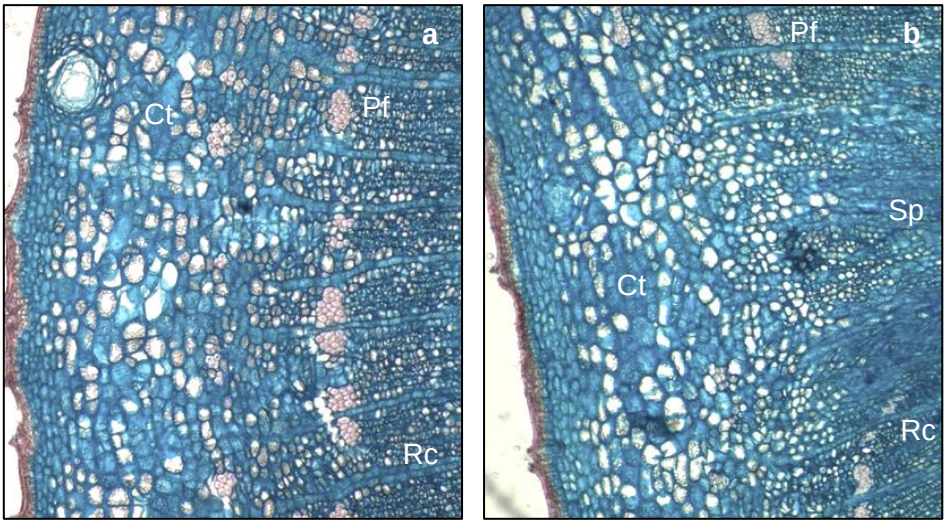

Fig. 1. Phloem-associated tissue in unaffected (a) and pitted (b) portions of T3-KB-infected 'Mexican' lime thin sections, stained with Safranin O and Alcian Blue 8GX. Ct – Cortex; Pf – phloem fibers; Rc – ray cells; Sp – stem pitting-affected tissue

The normal arrangement of phloem elements was disrupted in the case of stem pitting (Fig. 1b). The unorganized mass of cells at the cambial zone and the disruption of the normal ring of lignified phloem fibers (light-red bundles) is evident compared to unpitted tissue (Fig. 1a) and is consistent with previous findings (Brlansky et al., 2002; Sun and Folimonova, 2022). The connection between the phloem companion cells (surrounding the phloem fibers) and the ray cells is also apparent in the unpitted stem portion (Fig 1a). In the case of CTV stem pitting, this has recently been proposed as a potential virus transport route from its principle replication niche in phloem parenchyma and companion cells to the undifferentiated xylem tissue deeper within the stem (Sun and Folimonova, 2022).

The xylem-associated tissue in stem pits was also examined using biological staining. The wedge-like morphology of the pitted xylem tissue in 'Mexican' lime (Fig. 2a) closely resembles that of the stem pits observed in 'Star Ruby' grapefruit plants, as seen using high-resolution computed tomography (HRCT) scanning (Aldrich et al., 2021). The impacted xylem tissue was unlignified (blue) compared to the normally differentiated surrounding tissue. The living ray parenchyma cells could be identified in stained thin sections as unlignified (blue) cells with a regular and continuous dispersion throughout the width of the stem, radiating from the central pith. Based on color intensity and relative cell morphology, the impacted xylem tissue most closely resembled the living ray cells within the woody portion of the stem (darker blue). Phloem tissue stained light blue, as was expected owing to its unlignified, globular nature.

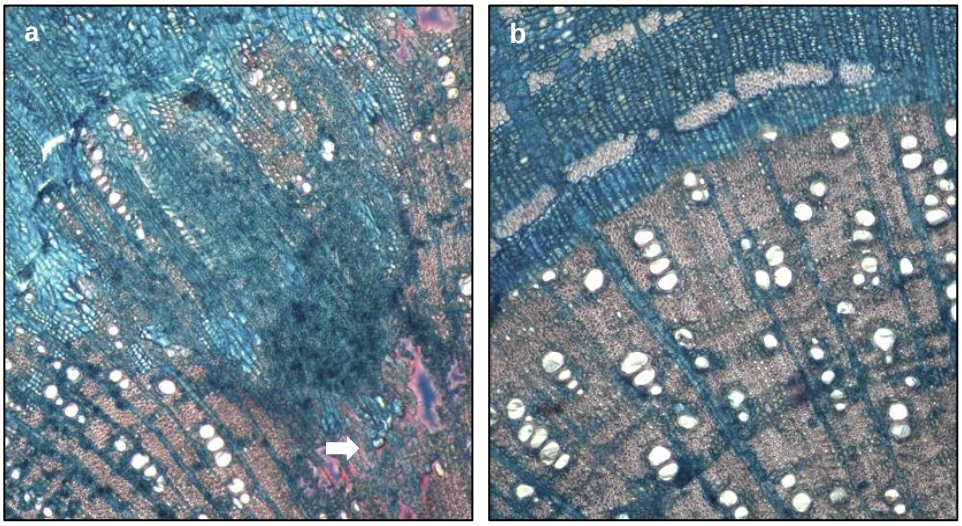

Fig. 2. Histological staining of citrus thin sections using Safranin O and Alcian Blue. Unlignified xylem tissue towards the inside of the stem pit can be seen in the pitted portion of a T3-KB-infected 'Mexican' lime plant (a) compared to an unpitted region (b). (Red –lignified; Blue – unlignified)

Interestingly, there were clusters of cells deep within the stem pits (white arrow – Fig. 2a) that resembled phloem-associated cells more so than ray cells and xylem parenchyma, as is the case in the majority of the stem pit. These cells are large and globular in shape and have similar staining behavior as the phloem tissue, seen on the periphery of the section (Fig. 2a). A possible explanation for this is that the initial perturbance of the vascular cambium at the stem pitting site triggered a chain reaction of dedifferentiation of these cells as the plant expands radially. The absence of proper cambium regulation at these sites could have caused the phloem-associated cells to remain at the initial site of perturbance. The xylem elements (tracheids, xylem parenchyma, ray cells, and vessel elements) surrounding these cells grow normally, while there is a deposition of unorganized parenchymatic tissue above the disruption site to compensate for the lack of normally differentiated tissue. This would be analogous to scar tissue in mammalian systems.

Sun and Folimonova (2022) recently proposed a four-stage process of CTV colonization into vascular tissue and subsequent stem pitting formation from time-course observations using a GFP-tagged CTV infectious mutant clone. The authors noted hypertrophic, irregularly shaped virus-colonized cells at the initial sites of xylem colonization (Sun and Folimonova, 2022). The morphological characteristics of the clusters of seemingly phloem-associated cells deep within the pitted xylem tissue observed in this study seem to match that description. It was of interest, however, that the cells that comprise the stem pit had an array of different morphological characteristics and were distinguishable based on Safranin O and Alcian Blue staining (Fig. 2 a). The impacted xylem tissue in cases of CTV-induced stem pitting has previously been referred to as 'yellow gumming material' or 'gumming malformations' (Brlansky et al., 2002; Sun and Folimonova, 2022). The results obtained from the conducted staining would suggest that the 'gumming material' observed here was heterogeneous in nature, consisting of a combination of different cell types.

Serial block face scanning electron microscopy

To characterize the three-dimensional aspects of xylem tissue impacted by stem pitting, the utility of the 3DEM technique, serial block face scanning electron microscopy (SBF-SEM) was evaluated.

Compared to softer biological samples, the hard nature of the woody tissue and the large size of stem pits potentially complicate the sectioning and rendering of samples conductive, as has been reviewed and reported in other SBF-SEM work on bone tissue (Goggin et al., 2020). The sample preparation pipeline for stem pitting characterization, therefore, needed to be optimized to overcome these potential issues. Firstly, the sub-sectioning of single stem pits before embedding allowed for a smaller tissue size starting point (Fig. 3b). By first visualizing the unembedded sample under low-vacuum SEM, the region of interest (ROI) could be identified, which facilitated further sample trimming and cutting of a reference corner (Fig. 3c and d). The heavy metal staining within the sample preparation protocol renders the tissue very dark (Fig. 3e), making structures difficult to distinguish.

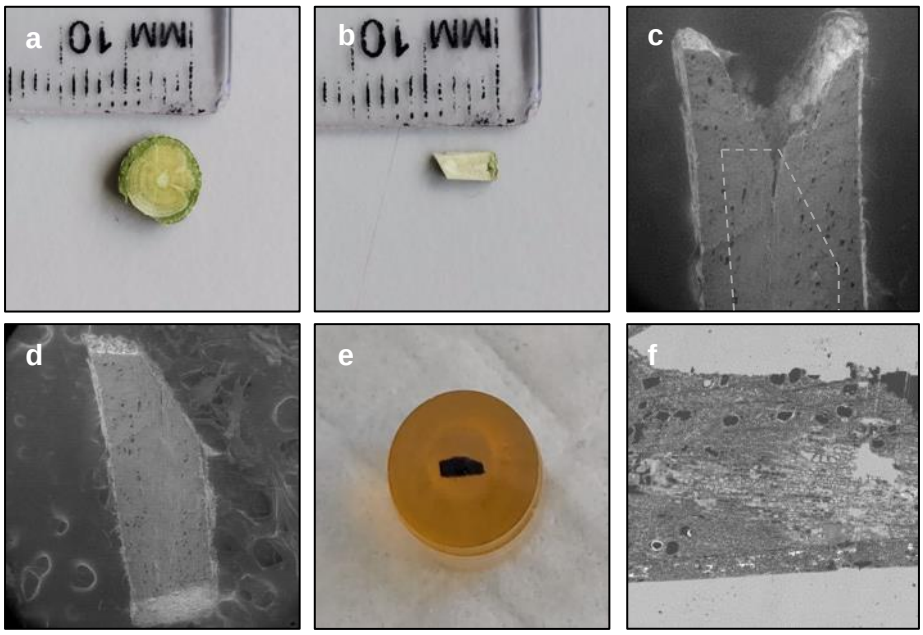

Fig. 3. Serial block face scanning electron microscopy sample preparation workflow. (a) – citrus stem section with stem pits visible; (b) – Hand-sectioned single stem pit; (c) – Low-vacuum scanning electron micrograph of sectioned stem pit after removal of the bark layer (the region to be retained following trimming is shown by the dotted line); (d) – Scanning electron micrograph of stem pit following additional trimming and reference corner cutting; (e) – Stained and resin-embedded sample; (f) – High-resolution scanning electron micrograph of 100 nm transverse thin section on a silicon nanowafer of pitted xylem tissue for region of interest (ROI) validation.

The next step was to establish whether the entire area of xylem tissue comprising the stem pit could be imaged in the SBF-SEM process. Fig. 4 shows the full high-resolution image of the affected xylem tissue of a single 'Mexican' lime stem pit. Three separate image stacks (tile stacks) were generated to span the entire length of the stem pit and were stitched together using the Amira software package (Thermo Fisher, Netherlands).

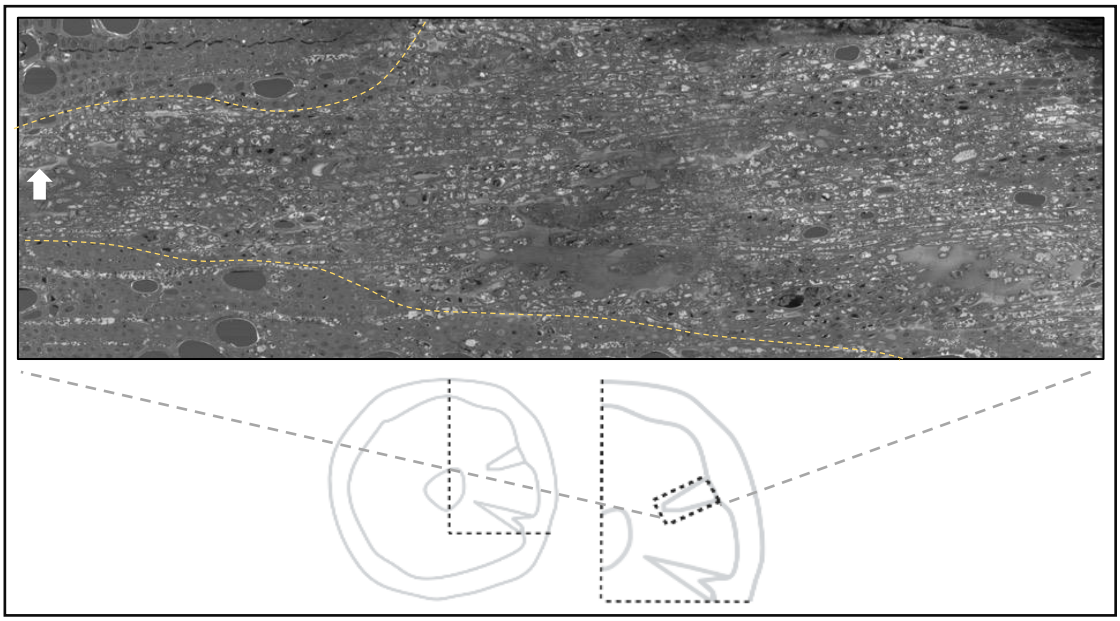

Fig. 4. SBF-SEM cross-section of the entire length of a stem pit in CTV T3-KB-infected 'Mexican' lime plant. The white arrow denotes the innermost point of the stem pit (middle-left) with normally differentiated xylem tissue to the top and bottom. The top right side of the image shows the periphery of the woody tissue. A diagrammatical representation of the stem portion portrayed in Fig. 3a is provided to place the stitched SBF-SEM image in context. The boundaries of the stem pitting-affected tissue are delineated by the dotted lines.

The impacted cells in the stem pit are distinguishable from the surrounding xylem tissue based on cell shape and size. There are indications of normal, functional xylem vessel elements and tracheids within the stem pit, though in very low abundance, highlighting how transport of water, minerals, and carbohydrates would be impaired by stem pitting leading to reduced tree vigor (Brlansky et al., 2002). The presence of some functional xylem elements within the pitted xylem tissue is consistent with recent findings by Sun and Folimonova (2022) who employed toluidine blue staining on citrus thin sections impacted by CTV stem pitting.

To compare the morphological properties of the affected xylem cells to the normally differentiated tissue surrounding it, the innermost portion of the stem pit was focused on. Fig. 5 illustrates the different cell types that comprise the stem pit at a higher magnification and unpitted tissue for comparison.

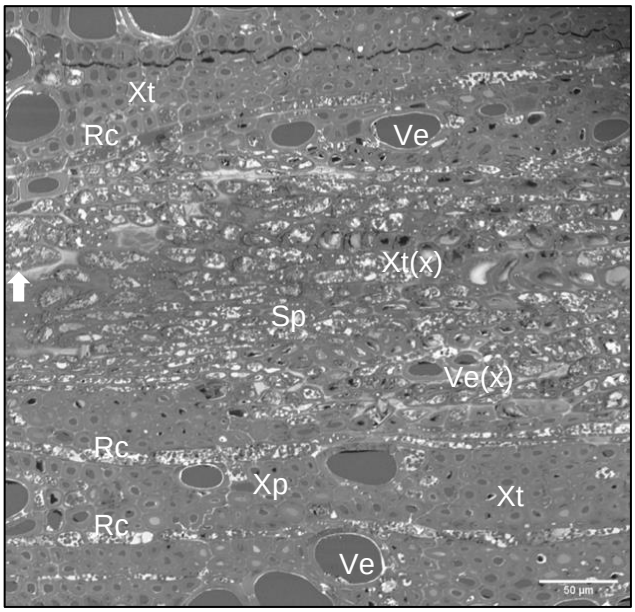

Fig. 5. SBF-SEM cross-section through pitted xylem tissue in a resin-embedded 'Mexican' lime sample. Sp – Stem pitting-affected tissue; Xt - xylem tracheid; Ve - vessel element; Rc – living ray cell; Xp – xylem parenchyma; Xt(x) - xylem tracheid within stem pit; Ve(x) – vessel element within stem pit. A 50 µm scale bar is provided in the bottom-right corner.

Normally differentiated xylem tracheids (Xt) and vessel elements (Ve) can be seen at the top and bottom of the impacted cells, which occupy the middle third of the image. The regular arrangements of living ray cells (Rc) are also apparent within the unpitted tissue to the top and bottom of the stem pit. The cells within the stem pit appear parenchymatic (undifferentiated) and disorganized in size, shape, and orientation to one another. There is a broad range of different cell sizes visible within the stem pit, corroborating the heterogeneous nature of pitted xylem tissue seen using biological staining (Fig. 2a). The impacted tissue also appears living as it has cytoplasmic contents, similar to what is observed in the living ray cells (Rc) and the xylem parenchyma (Xp). This highlights how CTV replication could be facilitated here and observed deep within the woody tissue. Similar to what was observed in the biological staining (Fig. 2a), there are large, globular cells at the innermost point of the stem pit (Fig. 5 - white arrow) compared to the surrounding pitted tissue. These cells could be similar to the virus-colonized, hypertrophic cells at the initiation sites of CTV xylem invasion, as noted by Sun and Folimonova (2022). The presence of these cells deep within stem pits could indicate that they were likely initially infected with CTV and remained undifferentiated at their initial location, while radial growth and stem pitting development progressed peripherally over time. The stack of high-resolution SEM images of this region highlighted the range of different cell shapes and their relative orientation within the stem pit, as well as how these structures changed as the sectioning and imaging of the stem pit progressed. A cross-sectional video of this image stack could be generated, highlighting these changes.
(https://www.youtube.com/watch?v=JdV-UikCEvI).

For comparison and potential classification of the impacted xylem cells, morphometric analysis was conducted using the software package, Fiji. Cell walls of the different cell types present within the pitted cross section (Fig. 5) were measured using the 50 µm scale bar. Twenty measurements of each cell type were made, and the results are illustrated in Fig. 6.

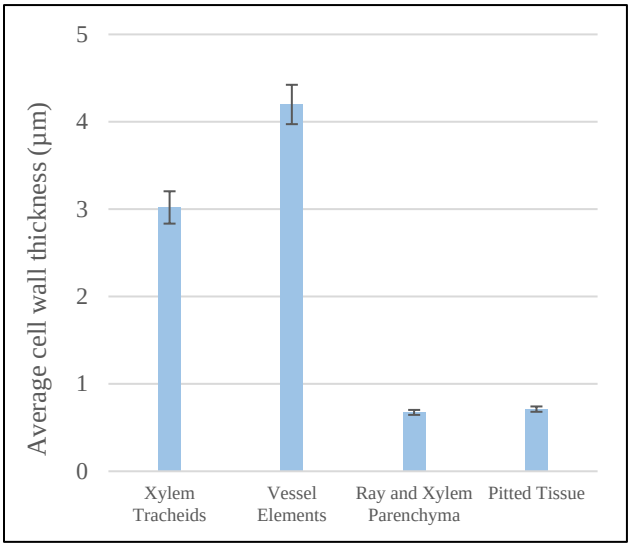

Fig. 6. Morphometric comparison of the average cell wall thickness of the different cell types within the impacted xylem tissue of a CTV T3-KB infected 'Mexican' lime plant. Twenty measurements per cell type were made. Bars indicate standard error.

Based on the cell wall thickness measurements the pitted cells most closely resembled the xylem parenchyma and living ray cells, further corroborating their unlignified status as seen using biological staining as well (Fig. 2a). The cell walls of the xylem tracheids and vessel elements were significantly thicker than that of the xylem parenchyma and ray cells. This was expected due to their highly lignified (thickened) secondary cell walls compared to parenchymatic tissue, which lacks secondary cell wall deposition (Sun and Folimonova, 2019). Cell sizes were additionally measured and compared for further classification of pitted cells in comparison to normally differentiated surrounding cell types. By making use of the image stack, cell measurements were made in the middle of cells in each case to ensure consistency. All "length" measurements denote measurements made from left to right, while "width" was measured from top to bottom, relative to the orientation of the cell in each case. Twenty measurements per cell type were made, and the results are illustrated in Fig. 7.

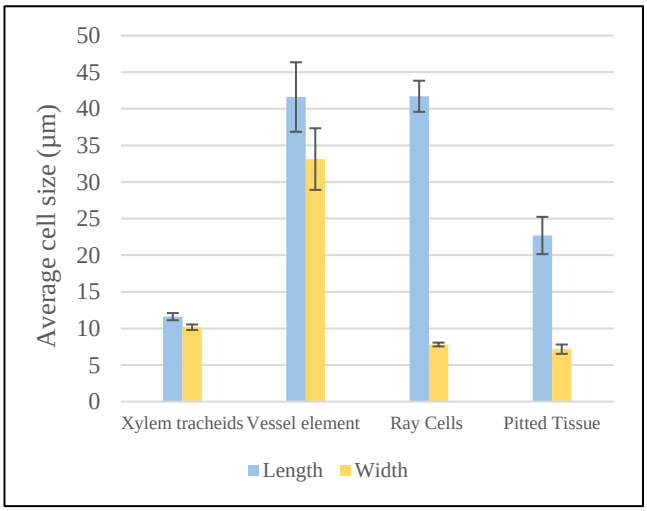

Fig. 7. Morphometric comparison of stem pitting-affected cell sizes within the impacted xylem tissue of a CTV T3-KB infected 'Mexican' lime plant. The range of different cell sizes within a stem pit ('Pitted Tissue') were measured and compared to the normally differentiated surrounding xylem elements observed within the same image stack. Twenty measurements per cell type were made. Bars indicate standard error.

As expected, the xylem tracheids and vessel elements had comparable length and width measurements in each case owing to their uniform, tube-like morphologies. Ray cell measurements confirmed their elongated shape and consistent width. Based on the visual and morphometric assessments, the pitted cells most closely resemble the ray parenchyma within the image stack, as was also seen by comparing the color intensity of the stem pit using biological staining (Fig. 2a). The variation between measurements of pitted cells, in particular the width measurements, was greater than that seen in the ray cell measurements. This supports the heterogeneous nature of the impacted xylem tissue comprising a wide range of cell shapes and sizes, seen by visual assessment as well. To further characterize these cells, three-dimensional software renderings of tissues of interest were generated and overlayed onto the original image map. Fig. 8 illustrates the 3D renderings of select cell types for comparison.

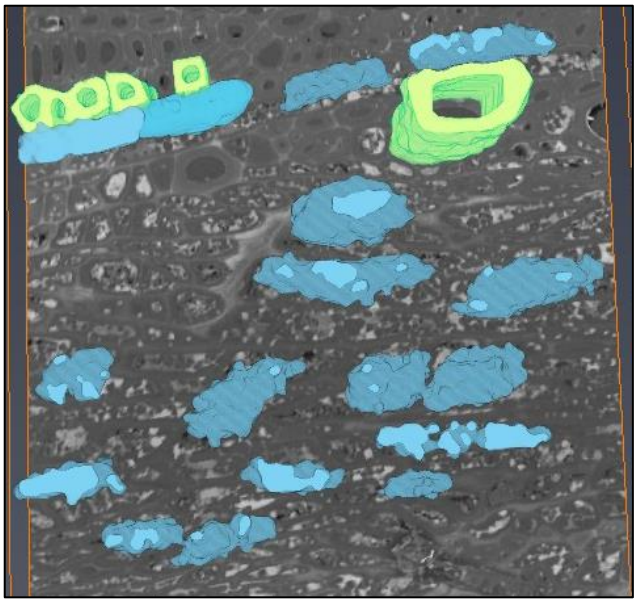

Fig. 8. Three-dimensional rendering of cell types in SBF-SEM image stack. Parenchymatic tissue (ray cells and pitted xylem cells) is in blue, and xylem tracheids and a vessel element are in green.

The 3D renderings illustrated in Fig. 8 confirm the wide variety of cell morphologies within the stem pitting-affected xylem tissue. Cells range from having a large, globular shape, to being very small and elongated, with a spectrum of shapes in between. The normally differentiated xylem elements (tracheids, ray cells, and a vessel element) are illustrated at the top of the image. The vessel elements and tracheids are highlighted in green, with the continuous row of ray parenchyma running in between, highlighted in light blue. The graphical renderings also support the notion that the pitted cells most closely resemble the adjacent ray parenchyma tissue. A cross-sectional video in which rendered elements appear as the software pans through the z-axis of the image stack was generated and provided a unique view of the shapes and orientations of impacted cells in comparison to adjacent tissue. (https://www.youtube.com/watch?v=Z9NxCa76MTQ)

Some functional tracheids and vessel elements within the pitted tissue were also apparent in the innermost tile stack evaluated here. By assessing the stack by panning through the sample along the z-axis, it appeared as though the shapes of these transport elements were warped by the mass of undifferentiated, parenchymatic tissue surrounding it. A single tracheid within the stem pit was mapped and rendered three-dimensionally to evaluate this graphically. Fig. 9 shows the 3D rendering of an impacted xylem tracheid compared to unaffected tracheids and a vessel element situated outside the stem pit.

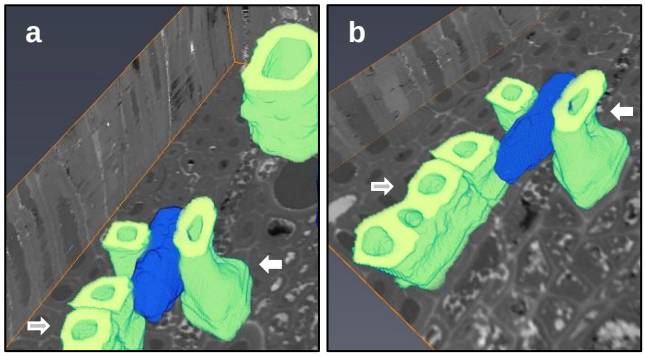

Fig. 9. Three-dimensional rendering of impacted xylem tracheid (white arrow) in SBF-SEM image stack in comparison to unaffected neighboring xylem tracheids (grey arrow). A single ray cell (dark blue) is situated between the xylem tracheids. A normally differentiated vessel element is also shown (a). Two angles (a and b) are provided to highlight the effect on the tracheid morphology.

The graphical rendering of the impacted xylem tracheid in Fig. 9 provided a novel, three-dimensional view of how the structure of this tissue was compromised within the stem pit. Changes in the structure of tracheary elements could likely have a negative effect on their functioning as the structure and function of the xylem are closely linked (Venturas et al., 2017). In more severe cases, CTV stem pitting causes stunted plant growth and the production of small, unmarketable fruit, which is thought to result from a restriction in water and nutrient transport (Tatineni and Dawson, 2012). The results of this study suggest that the negative impact of stem pitting on vascular transport in affected plants likely results from the low abundance of transport elements observed within the pitted xylem tissue, as well as structural abnormalities that may negatively influence their functionality.

In this proof-of-concept study, the novel technique of SBF-SEM was successfully used to study the xylem-associated cells in stem pitted tissue. To our knowledge, this is the first instance of a 3DEM technique being used for plant disease characterization in hard, woody materials. Morphometric and visual comparisons were conducted, and xylem cells impacted by stem pitting were determined to be disorganized in size, shape, and orientation. These cells were also found to resemble the living ray parenchyma cells most closely in the adjacent portions of the stems. The three-dimensional renderings of cells of interest yielded useful graphical representations of the impacted tissue and facilitated the comparisons and classifications made. The results obtained complemented recent findings of CTV-induced stem pitting in citrus (Sun and Folimonova, 2019, 2022). The stem pitting in this study was caused by a wild-type CTV infection (CTV T3-KB), and follow-up work using GFP-tagged infectious clones to induce different stem pitting phenotypes could prove valuable. By combining fluorescent microscopy with SBF-SEM analyses to study stem pits induced by these infectious clones, one can further confirm which of the affected xylem-associated cells in stem pits play host to CTV. There are also opportunities for combining non-destructive technologies such as HRCT and SBF-SEM, to complement the analyses and facilitate region finding, as has been demonstrated on a variety of biological samples by Starborg et al. (2019). Further refinement of SBF-SEM applications to characterize CTV-induced stem pitting could yield insights on disease induction and progression, with particular reference to evaluating distinct stem pitting phenotypes in different citrus hosts. This can aid in determining if different stem pitting phenotypes result from distinct plant-pathogen interactions or if there is a universal stem pitting response in CTV-infected citrus.

Acknowledgments

The financial assistance of the National Research Foundation (NRF) towards this research is hereby acknowledged. Opinions expressed and conclusions arrived at, are those of the authors and are not necessarily to be attributed to the NRF. This research was funded by Citrus Research International (CRI Project 1160).

References

Aldrich, D.J., Bester, R., Cook, G., Du Plessis, A., Burger, J.T., Maree, H.J., 2021. Evaluating high-resolution computed tomography to study citrus tristeza virus-induced stem pitting. J. Citrus Pathol. 8. https://doi.org/10.5070/C481050093

Brlansky, R.H., Howd, D.S., Broadbent, P., Damsteegt, V.D., 2002. Histology of sweet orange stem pitting caused by an Australian isolate of Citrus tristeza virus. Plant Dis. 86, 1169–1174.

Dawson, W.O., Garnsey, S.M., Tatineni, S., Folimonova, S.Y., Harper, S.J., Gowda, S., 2013. Citrus tristeza virus-host interactions. Front. Microbiol. 4. https://doi.org/10.3389/fmicb.2013.00088

Denk, W., Horstmann, H., 2004. Serial Block-Face Scanning Electron Microscopy to Reconstruct Three-Dimensional Tissue Nanostructure. PLoS Biol. 2, e329. https://doi.org/10.1371/journal.pbio.0020329

Eustaquio, T., Wang, C., Dugard, C.K., George, N.I., Liu, F., Slikker, W., Paule, M.G., Howard, P.C., Paredes, A.M., 2018. Electron microscopy techniques employed to explore mitochondrial defects in the developing rat brain following ketamine treatment. Exp. Cell Res. 373, 164–170. https://doi.org/10.1016/j.yexcr.2018.10.009

Folimonova, S.Y., 2013. Developing an understanding of cross-protection by Citrus tristeza virus. Front. Microbiol. 4. https://doi.org/10.3389/fmicb.2013.00076

Garnsey, M., SM, G., EL, L., others, 1987. Toward a standardized evaluation of the biological properties of citrus tristeza virus. Phytophylactica 19, 151–158.

Goggin, P., Ho, E.M.L., Gnaegi, H., Searle, S., Oreffo, R.O.C., Schneider, P., 2020. Development of protocols for the first serial block-face scanning electron microscopy (SBF SEM) studies of bone tissue. Bone 131, 115107. https://doi.org/10.1016/j.bone.2019.115107

Helmstaedter, M., Briggman, K.L., Denk, W., 2008. 3D structural imaging of the brain with photons and electrons. Curr. Opin. Neurobiol. 18, 633–641. https://doi.org/10.1016/j.conb.2009.03.005

Hughes, L., Hawes, C., Monteith, S., Vaughan, S., 2014. Serial block face scanning electron microscopy—the future of cell ultrastructure imaging. Protoplasma 251, 395–401. https://doi.org/10.1007/s00709-013-0580-1

Lewis, A.J., Genoud, C., Pont, M., van de Berg, W.D., Frank, S., Stahlberg, H., Shahmoradian, S.H., Al-Amoudi, A., 2019. Imaging of post-mortem human brain tissue using electron and X-ray microscopy. Curr. Opin. Struct. Biol. 58, 138–148. https://doi.org/10.1016/j.sbi.2019.06.003

Lott, T.B., Keane, F.W.L., May, J., 1962. Gumming, distortion, and pitting in cherry and apricot. Can. Plant Dis. Surv. 42, 229–232.

Marini, D.B., Zhang, Y.-P., Rowhani, A., Uyemoto, J.K., 2002. Etiology and Host Range of a Closterovirus Associated with Plum Bark Necrosis-Stem Pitting Disease. Plant Dis. 86, 415–417. https://doi.org/10.1094/PDIS.2002.86.4.415

Martelli, G.P., Adams, M.J., Kreuze, J.F., Dolja, V.V., 2007. Family Flexiviridae: A Case Study in Virion and Genome Plasticity. Annu. Rev. Phytopathol. 45, 73–100. https://doi.org/10.1146/annurev.phyto.45.062806.094401

Moreno, P., Ambros, S., Albiach-Martí, M.R., Guerri, J., Pena, L., 2008. Citrus tristeza virus: a pathogen that changed the course of the citrus industry. Mol. Plant Pathol. 9, 251–268. https://doi.org/10.1111/j.1364-3703.2007.00455.x

Ornelas, S., Berthiaume, A.-A., Bonney, S.K., Coelho-Santos, V., Underly, R.G., Kremer, A., Guérin, C.J., Lippens, S., Shih, A.Y., 2021. Three-dimensional ultrastructure of the brain pericyte-endothelial interface. J. Cereb. Blood Flow Metab. 41, 2185–2200. https://doi.org/10.1177/0271678X211012836

Pallas, V., García, J.A., 2011. How do plant viruses induce disease? Interactions and interference with host components. J. Gen. Virol. 92, 2691–2705. https://doi.org/10.1099/vir.0.034603-0

Smith, D., Starborg, T., 2019. Serial block face scanning electron microscopy in cell biology: Applications and technology. Tissue Cell 57, 111–122. https://doi.org/10.1016/j.tice.2018.08.011

Smith, S.H., Stouffer, R.F., Soulen, D.M., 1973. Induction of stem pitting in peaches by mechanical inoculation with Tomato ringspot virus. Phytopathology 63, 1404–1406.

Srebotnik, E., Messner, K., 1994. A Simple Method That Uses Differential Staining and Light Microscopy To Assess the Selectivity of Wood Delignification by White Rot Fungi. Appl. Environ. Microbiol. 60, 1383–1386. https://doi.org/10.1128/AEM.60.4.1383-1386.1994

Starborg, T., O'Sullivan, J.D.B., Carneiro, C.M., Behnsen, J., Else, K.J., Grencis, R.K., Withers, P.J., 2019. Experimental steering of electron microscopy studies using prior X-ray computed tomography. Ultramicroscopy 201, 58–67. https://doi.org/10.1016/j.ultramic.2019.03.002

Sun, Y., Folimonova, S.Y., 2022. Location matters: from changing a presumption about the Citrus tristeza virus tissue tropism to understanding the stem pitting disease. New Phytol. 233, 631–638. https://doi.org/10.1111/nph.17777

Sun, Y., Folimonova, S.Y., 2019. The p33 protein of Citrus tristeza virus affects viral pathogenicity by modulating a host immune response. New Phytol. 221, 2039–2053. https://doi.org/10.1111/nph.15482

Sun, Y.-D., Spellman-Kruse, A., Folimonova, S.Y., 2022. Blaze a New Trail: Plant Virus Xylem Exploitation. Int. J. Mol. Sci. 23, 8375. https://doi.org/10.3390/ijms23158375

Tapia, J.C., Kasthuri, N., Hayworth, K.J., Schalek, R., Lichtman, J.W., Smith, S.J., Buchanan, J., 2012. High-contrast en bloc staining of neuronal tissue for field emission scanning electron microscopy. Nat. Protoc. 7, 193–206. https://doi.org/10.1038/nprot.2011.439

Tatineni, S., Dawson, W.O., 2012. Enhancement or Attenuation of Disease by Deletion of Genes from Citrus Tristeza Virus. J. Virol. 86, 7850–7857. https://doi.org/10.1128/JVI.00916-12

Venturas, M.D., Sperry, J.S., Hacke, U.G., 2017. Plant xylem hydraulics: What we understand, current research, and future challenges. J. Integr. Plant Biol. 59, 356–389. https://doi.org/10.1111/jipb.12534

Welsh, M.F., May, J., 1966. Virus induced wood pitting in the root systems of apple seedlings, and its effects on tree vigor. Can. J. Plant Sci. 47, 51–59.